PROCEEDINGS, 47th Workshop on Geothermal Reservoir Engineering
Stanford University, Stanford, California, February 7-9, 2022
SGP-TR-223

Pressure Transient Analysis of Injection/Fall-off Tests in the Geothermal Reservoirs with Free CO_2 Phase

Gitta A. Septiani[1,2] and Eylem Kaya[1]

[1]Department of Engineering Science, The University of Auckland, Private Bag 90210, Auckland, New Zealand
[2]PT Sarana Multi Infrastruktur, Jakarta, Indonesia

gsep095@aucklanduni.ac.nz, e.kaya@aucklanduni.ac.nz

Keywords: Pressure transient analysis, numerical models, geothermal well testing, free CO_2 phase geothermal reservoir, injection/fall-off test

ABSTRACT

Non-condensable gases consisting primarily of CO_2 are commonly found in geothermal fluids. As the expansion and compression of CO_2 can occur during the well test, those conditions further complicate the analysis of geothermal well test data. Early analytical methods for pressure transient analysis (PTA) commonly assume that the reservoir contains single-phase flow and slightly compressible fluids. However, in CO_2-rich geothermal fields, the pressure transient testing in the geothermal reservoir involves a complex process of heat transfer, flow of multi-phase and multi-component conditions. This study examines the response of geothermal reservoirs that initially contains the free CO_2 phase to injection/fall-off tests. Numerical modelling was carried out by using TOUGH2 simulator. Key parameters in the multi-phase geothermal reservoirs such as gas saturation and relative permeability were also investigated to identify their effect on the characteristic appearance in the derivative plots. The results illustrate that a pressure decline is observed in a log-log pressure derivative plot before reaching the infinite-acting radial flow due to the dissolution of CO_2 in the reservoir during single-phase pure water injection. The pressure responses were then analyzed using analytical models to estimate the reservoir properties. Furthermore, the estimated reservoir properties were compared with the actual values inputted to TOUGH2 to identify variables that may mislead the interpretation of the reservoir characteristics. Thus, the results provide insights into the interpretation of PTA data from CO_2-rich fields.

1. INTRODUCTION

Pressure transient analysis (PTA) is a crucial step in developing geothermal systems economically due to its ability to interpret the reservoir characteristics by analyzing the pressure response data from the well testing. However, analytic models developed for PTA in early times have basic assumptions that the reservoir is single phase, has relativity low temperature, and has a simple geological structure as it was mainly developed for petroleum and groundwater applications. These assumptions contradict with the geothermal reservoir as it has complex non-isothermal, non-uniform situations, non-linear fluid properties, and phase changes (McLean & Zarrouk, 2017; O'Sullivan & McKibbin, 1989).

The presence of free CO_2 in the two-phase reservoir complicates the pressure transient analysis in geothermal applications as it significantly affects the thermodynamic condition and the results of a well test. The mass fractions of CO_2 in the liquid and gas phase (a mixture of H_2O and CO_2) depend on the temperature and pressure. In moderately high partial pressure of CO_2, the total amount of CO_2 that can be dissolved in the liquid phase is small, and if it is larger, the mixture of H_2O and CO_2 must boil and evolve into the gas phase (O'Sullivan et al., 1983). In geothermal systems, the mass of CO_2 in the gas phase is larger than in a unit volume of liquid phase. If CO_2 partial pressure is kept at a constant value, an increase of CO_2 mass fraction is accompanied by an increase in gas-phase saturation. This will result in the total mixture mobility as it depends on the volumetric fractions of the liquid and gas phase (O'Sullivan et al., 1983).

Numerous studies have recognized the limitation of PTA analytic models and utilized the numerical modelling of PTA using TOUGH2 (Adityatama et al., 2018a,b; Guerra & O'Sullivan, 2018; McLean & Zarrouk, 2017). TOUGH2 has been widely used in simulating the non-isothermal flows of multi-component, multi-phase fluids in one-, two-, and three-dimensional porous and fractured media (Pruess et al., 1999). Adityatama et al., (2018a) examined the CO_2 effects on injection/fall-off cases. It showed that by varying the CO_2 content, the pressure response of the reservoir is similar where CO_2 is dissolved inside the geothermal fluid. Beyond that, the CO_2 becomes free inside the reservoir, and the pressure response is different from the model of dissolved CO_2. Using semilog calculation, the attempt to calculate the reservoir properties overestimated the reservoir permeability and skin factor. Kaya et al., (2019) further analyzed the CO_2 effects during the drawdown/build-up test. Similar to the injection/fall-off cases, the dissolved CO_2 model gave a similar result as the pure water model. However, if the pressure drops below the boiling point or CO_2 is released from the fluid, it will alter the pressure response resulting in the unrecognized pressure derivative plot. The semilog calculation can be used to estimate the reservoir if the unit slope and flat line can be recognized.

This study investigates the numerical pressure transient analysis of injection/fall-off test under the various conditions of a geothermal reservoir such as single-phase pure water and reservoir with free CO_2 phase. The effect of injectate temperature in the injection/fall-off test is also investigated in this study to identify how temperature changes affect the results of PTA and to decide appropriate fluid properties depending on the reservoir and test conditions. Moreover, this study examines the boundary conditions that control the reservoir pressure

response which are closed (no-flow) boundary and constant pressure boundary. Therefore, the results of this study may be used in an attempt to identify any undesirable sensitivities and interpret the real pressure transient data from the geothermal fields more accurately.

AUTOUGH2 simulator was used for numerical modelling of non-isothermal flows of multi-component, multi-phase fluids in porous media (Yeh et al., 2012). Also, the PyTOUGH scripting library was used for automation TOUGH2 setup and simulation (Croucher, 2011). Furthermore, the TIM graphical tool was utilized for assisting in visualizing the results from TOUGH2 simulations (Yeh et al., 2012). The analytical PTA methods used in this study are manual calculations and plotting of Horner and semilog plots, log-log plots of pressure (Bourdet et al., 1989; Onur & Al-Saddique, 1999; Zarrouk & McLean, 2019).

2. NUMERICAL MODEL SET UP

2.1 Model Geometry

The reservoir is represented by the radial model grid design shown in Table 1. In this study, the wellbore as part of porous media is not included for several reasons. First, early time behavior obtained from the numerical model results is sensitive to the parameters used in the well block (porosity, permeability, volume, compressibility values) and will affect the early time behavior of the numerical model. Second, if the well block is represented as porous media, it will appear as an additional skin factor effect. And the last one, geothermal systems are usually fractured, and the permeability of these fractures is very high. Unless it is a vapor-dominated system, we do not expect the wellbore storage period to be long in geothermal PTAs.

A well radius of 0.1 m was used to represent the empty space in the volume occupied by the wellbore. The skin zone has a high-resolution area immediately outside the wellbore at r direction. Outside the empty space of wellbore, the block sizes increase logarithmically until the radius of the region (skin, reservoir, or boundary) is achieved. Referring to previous numerical modelling of PTA work (McLean & Zarrouk, 2017; Septiani et al., 2021a,b), the pressure response is insensitive to the number of skin zone block and reservoir zone block.

Table 1: Key parameters for the 1D radial model

	Skin Zone	Reservoir Zone	Boundary Zone
Infinite Reservoir	• Radius = 3.875 m • Number of blocks = 14 blocks • Porosity = 0.1 • Permeability = 2 mD (positive skin); 100 mD (negative skin) • Skin factor = 14.63 (positive skin); -3.29 mD (negative skin)	• Radius = 132000 m • Number of blocks = 85 blocks • Porosity = 0.1 • Permeability = 10 mD (base) • Layer thickness = 600 m • Relative permeability = Linear; S_l = 0.3, S_v = 0.05	• Not applied
Reservoir Enclosed with Boundary	• Not applied	• Radius = 303.875 m (single phase model); 50 m (two-phase model) • Number of blocks = 99 blocks • Porosity = 0.1 • Permeability = 10 mD (base) • Layer thickness = 600 m • Relative permeability = Linear; S_l = 0.3, S_v = 0.05 (will be varied for two-phase model)	<u>Closed or No Flow Boundary</u> • No additional block <u>Constant Pressure Boundary</u> • Number of blocks = 1 block • Aquifer zone extent = 100 m (single phase model); 20 m (two-phase model) • Volume aquifer = 1 x 10^{99} m^3 • Nodal distance between reservoir and boundary blocks = 10^{-9} m

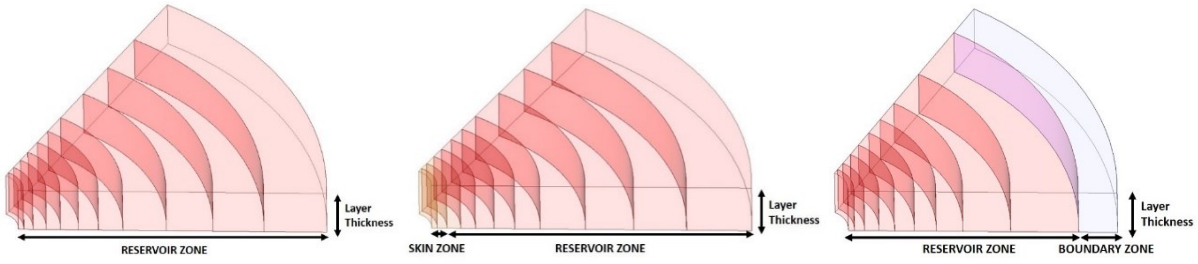

a. **b.** **c.**

Figure 1: Schematic of radial model grid setup; a. infinite reservoir; b. reservoir with a skin zone; c. reservoir with boundary zone

2.2 Base Model Parameters

For the single-phase reservoir model, Equation of State (EOS) 1 module of TOUGH2 is used, and the primary variables inputted are reservoir temperature of 250°C and reservoir pressure of 80 bar. To simulate the initial condition of a two-phase reservoir containing CO_2, EOS 2 module is used. The primary variables input for this condition is as follows (Pruess et al., 1999):

- P_g (gas phase pressure) = 80 bar

- S_g (gas saturation) = 3% (base model)
- PCO_2 (CO_2 partial pressure) = 40.197 bar (corresponds to the maximum concentration of dissolved CO_2 in an aqueous phase in accordance with reservoir pressure and temperature)

The gas phase pressure and temperature reservoir are 80 bar and 250°C, respectively. However, as the temperature is not inputted as the primary variables in EOS2, CO_2 partial pressure is used to define the initial temperature. This is because the partial pressure represents the amount of gas that dissolves at a particular temperature which depends on the pressure of the gas. The CO_2 partial pressure is calculated based on Henry's Law, given by:

$$P_{CO_2} = \frac{18}{44} \times K_h \times X_{CO_2} \quad (1)$$

Where Henry's Constant, K_h is calculated using a correlation from Battistelli et al., (1997), which extends the temperature range of Henry's constant correlation up to 350°C.

2.3 Model Test Set-Up

The injection/fall-off test is conducted with a single injection rate at the mass flow rate for 24 hours and the fall-off period lasting for 96 hours. To obtain accurate and realistic predictions for PTA problems, different reservoir parameters and various aspects of model design were investigated which are the effect of injectate temperature, negative and positive skin, and boundary conditions: no flow or closed and constant pressure. The key parameters in the multi-phase geothermal reservoirs, such as gas saturation and relative permeability, were also investigated. The following model schemes were examined:

- Reservoir zone (no-skin) extending infinitely
- Skin zone (positive and negative) and a reservoir zone, extending infinitely
- Reservoir zone (no-skin) with closed boundary
- Reservoir zone (no-skin) with constant pressure boundary

Table 2 summarizes the range model parameters tested in this study.

Table 2: Range tested for the injection/fall-off test in single-phase and two-phase with free CO_2 reservoir

Parameter and description	Range tested
Injectate temperature	57°C, 250°C
Skin zone permeability (skin factor)	2 mD (14.63), 100 mD (-3.29)
Boundary condition	No flow (closed) boundary, constant pressure boundary
Gas saturation	1%, 3%, 5%, 10%
Relative permeability	Linear; S_l = 0.3 S_v = 0.0; 0.03; 0.05; 0.1

3. SINGLE-PHASE PURE WATER MODEL

At first, a single-phase reservoir in 1D radial model is set up to obtain a generic model that can give reliable predictions for an injection/fall-off test and decide a reliable approximation for the non-uniform properties that are used for the investigation of PTA. Then, several tests are conducted on the model to investigate the sensitivity of the model results to several parameters that have been summarized in Table 2. The pressure derivative is plotted to illustrate the reservoir pressure response during the fall-off period. Moreover, the infinite acting radial flow regime (IARF) is identified and used to derive the reservoir properties using the manual calculation method (Horner and semilog plots). Δk represents the difference of permeability value between AUTOUGH2 inputs and the analytical model result; ΔSkin represents the difference in skin value between AUTOUGH2 inputs and the analytical model result.

3.1 Effect of Injectate Temperature

The effect of injectate temperature is simulated in the uniform reservoir that extends infinitely to observe the pressure response of the reservoir only without any other parameters that will affect the PTA result, such as skin zone or boundary. In this section, the pressure responses were observed during the injection and fall-off period and illustrated in Figure 2. The reservoir parameters estimated using Horner and semilog plots are shown in Table 3.

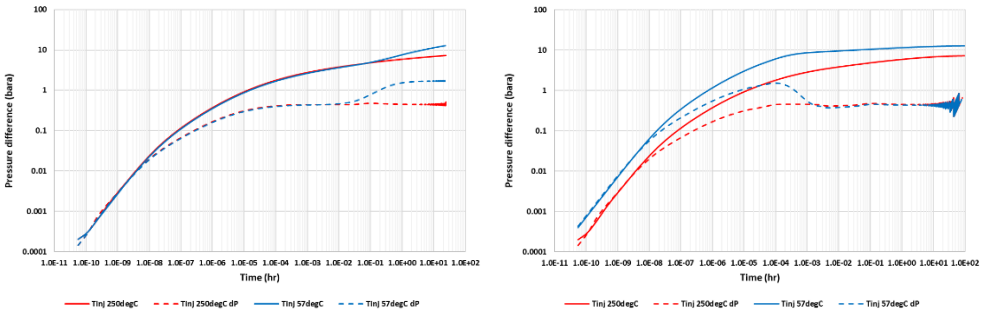

a. **b.**

Figure 2: Effect of injectate temperature on the pressure derivative plot in a reservoir (no-skin) extending infinitely; a. injectate temperature of 250°C; b. injectate temperature of 57°C

Table 3: Reservoir parameters estimated for different injectate temperatures in a reservoir (no-skin) extending infinitely

Injectate Temperature (°C)	k (mD)	Δk (mD)	Skin	ΔSkin
57	10	0	6.99	6.99
250	9.88	0.12	0.33	0.33

During the injection period (Figure 2a), the zero-slope straight line that indicates the infinite acting radial flow appears right after the transition time for the hot water injection case, while in the cold-water injection case, the zero-slope straight line appears twice. This is likely caused by the original reservoir fluid dominating the flow at the early radial flow, and then the cold injectate water occupies the second radial flow. The pressure and temperature response are plotted in a semilog plot (Figure 3) to derive the reservoir properties. It can be seen that the first radial flow observed is due to the reservoir fluid. Thus, the reservoir temperature properties are used to calculate the reservoir permeability. Then, the second radial flow occurs due to the injectate fluid. Accordingly, the injectate temperature properties are used to calculate the reservoir permeability.

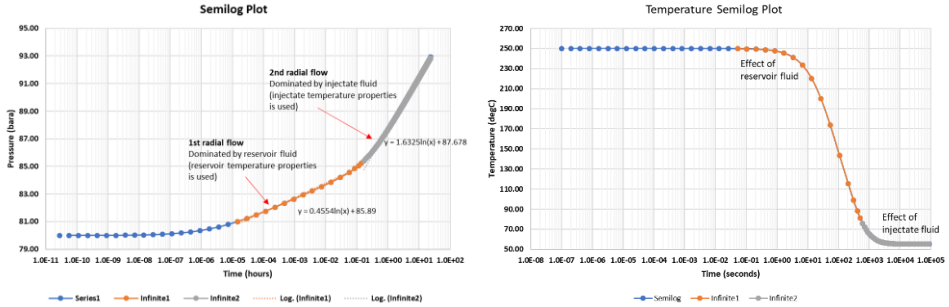

a. **b.**

Figure 3: a. Semilog plot for cold water injection; b. Temperature semilog plot for cold water injection

In the fall-off period (Figure 2b), the temperature difference between the injectate water and the reservoir fluid is apparent. This results in the derivative hump that resembles positive skin. This is due to the dependence of viscosity on temperature, as viscosity rapidly changes in the low temperature and less in the high temperature.

3.2 Effect of Skin Factor Value

The effect of skin condition is simulated by changing the permeability of the blocks in the skin zone. The derivative plot for the positive skin model is shown in Figure 4a, while Figure 4b illustrates the negative skin model.

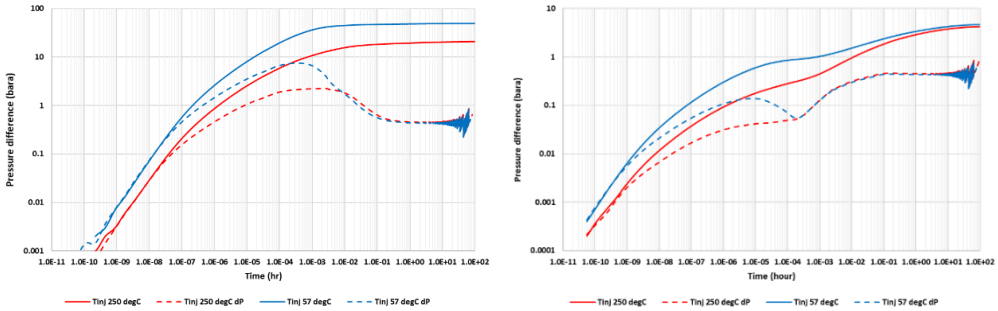

a. **b.**

Figure 4: Effect of skin factor value on the pressure derivative plot in a reservoir with skin zone extending infinitely; a. positive skin; b. negative skin

The derivative plot of positive skin (Figure 4a) shows the two models have similar curve shapes. However, in the 57°C injectate temperature case, the pressure derivative plot has a bigger hump than the 250°C injectate temperature case, showing that it has a higher skin factor value due to the bigger difference between injectate temperature and reservoir temperature. The derivative plot of negative skin (Figure 4b) illustrates that the two models have two humps. This might be the effect of negative skin as the permeability near the wellbore is higher than the reservoir permeability, resulting in the first hump being smaller than the second hump. The reservoir parameter estimation (Table 4) has an acceptable range of for permeability estimation but the skin factor value estimated for the 57°C injectate temperature case is greatly exaggerated.

Table 4: Reservoir parameters estimated for different injectate temperatures and skin factor values in the reservoir with skin zone extending infinitely

Actual skin factor value	Injectate temperature (°C)	k (mD)	Δk (mD)	Skin	ΔSkin
14.63 (positive skin)	57	10	0	46.72	32.09
	250	9.61	0.39	14.85	0.22
-3.29 (negative skin)	57	10.1	0.1	-2.26	1.03
	250	9.75	0.25	-3.05	0.24

3.3 Effect of Boundary Condition

A boundary can be defined as a surface positioned at a distance from the tested well where a flowing property changes (Houzé et al., 2012). In this study, we investigated two main boundary conditions that control the response of the reservoir to pressure changes: closed (no-flow) boundary and constant pressure boundary. To simulate the closed boundary condition, the radius of the reservoir is reduced to 300 m to intersect with a boundary zone, while for constant pressure boundary simulation, one block is added at the end of the radial model (after the reservoir zone) to simulate the huge aquifer that surrounded the circular model of the reservoir. The reservoir pressure response is plotted in the derivative plot shown in Figure 5.

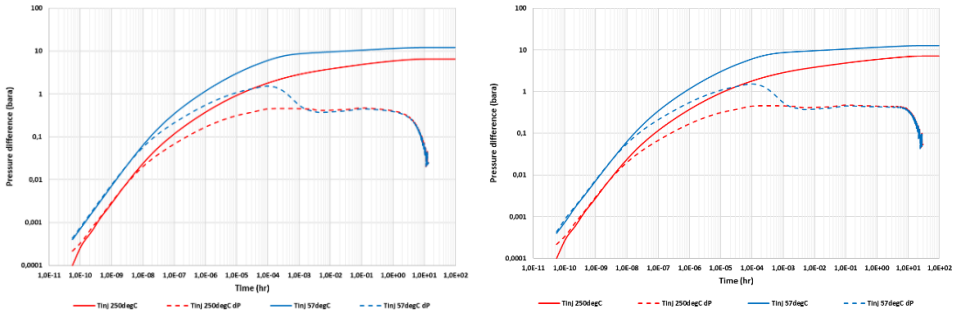

a. **b.**

Figure 5: Effect of boundary condition on the pressure derivative plot in a reservoir (no-skin) zone; a. closed or no flow boundary; b. constant pressure boundary

The derivative plot shows that the pressure derivative dives towards zero at the late times for both boundary conditions. The late time unit slope and pressure dip represent the pseudo-steady state flow as the fluid transfer back to the well zone until the pressure is stabilized back to the average reservoir pressure. The boundary effect is also investigated in the semilog analysis. For the closed boundary effect, the pressure response will go horizontally after the IARF and stabilized at the average reservoir pressure (Figure 6a). The pressure will also deviate from the IARF line flowing at constant pressure for the constant pressure boundary effect. However, the final pressure response is stabilized at the initial reservoir pressure at 80 bar (Figure 6b).

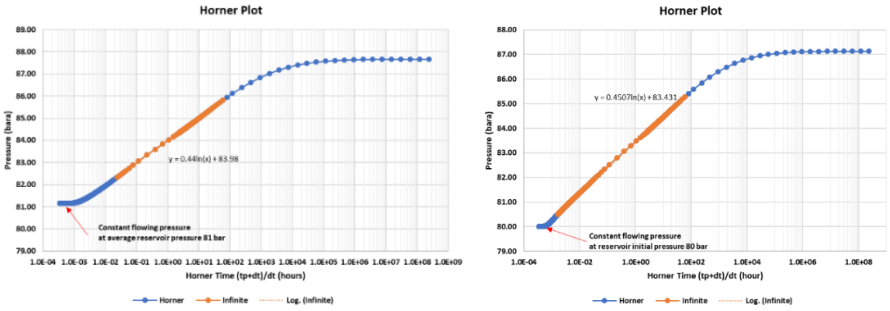

a. **b.**

Figure 6: Horner plot for fall-off period in a reservoir (no-skin) zone; a. closed or no flow boundary; b. constant pressure boundary

The reservoir parameter estimation for uniform reservoirs with a closed boundary is shown in Table 5. The permeability estimation is in acceptable range for both boundary conditions while it is overestimated for the low temperature injection case for skin estimation.

Table 5: Reservoir parameters estimated for different injectate temperatures and boundary conditions in the reservoir (no-skin) zone

Boundary condition	Injectate temperature (°C)	k (mD)	Δk (mD)	Skin	ΔSkin
Closed boundary	57	10.56	0.56	7.75	7.75
	250	10	0	0.53	0.53
Constant pressure boundary	57	9.94	0.06	7.05	7.05
	250	9.77	0.23	0.39	0.39

4. TWO-PHASE WITH FREE-CO2 MODEL

The presence of free CO_2 in the two-phase reservoir complicates the pressure transient analysis in geothermal applications. However, TOUGH2 can simulate the reservoir with NCG content as well as two-phase condition using EOS2. For a given gas phase pressure of 80 bar and temperature 250°C, the concentration of dissolved CO_2 in an aqueous phase can be a maximum of 1.98 wt%. The CO_2 partial pressure corresponding to this content is calculated as 40.197 bar. Thus, CO_2 partial pressure inputted in EOS2 is 40.197 bar to set the initial reservoir temperature to 250°C in TOUGH2, and this value will be used as initial CO_2 partial pressure in all model schemes experimented in this section. Furthermore, the numerical models will be set for a geothermal reservoir that initially has free CO_2 saturation, and the effect of the gas saturation and relative permeability was investigated, which the range tested is summarized in Table 2.

4.1 Effect of Gas Saturation

At first, the primary variables are inputted into the TOUGH2 and the initial condition at the start of the injection is observed. The observation is conducted to make sure that the reservoir initially has free CO_2 gas. According to the different gas saturations stated in Table 2, TOUGH2 has calculated how much CO_2 content was initially present in the reservoir. The results are shown in Table 6.

Table 6: Initial CO_2 content in the two-phase reservoir for different gas saturations

Gas saturation (%)	CO_2 content (%weight)
1%	2.00651%
3%	2.11084%
5%	2.21920%
10%	2.50940%

As shown in Table 6, the CO_2 content in the reservoir is above 1.98 wt%, representing that some of CO_2 gases are released as free gas in the reservoir and some of it is still dissolved in the reservoir fluid. In this section, the gas phase saturation is varied to observe the effect on the pressure derivative plot and to estimate the reservoir properties. The linear relative permeability curve is used with the immobile liquid saturation of 0.3 and immobile gas saturation of 0.05. The result is compared to the pressure response of single-phase reservoirs for further investigation.

4.1.1 Infinite reservoir with no skin

The gas saturation effect is simulated in the uniform reservoir that extends infinitely with different injectate temperatures. This simulation aims to know the pressure response of a free-CO_2-containing reservoir without considering any skin or boundary conditions affecting the PTA. The model simulation results are presented in the derivative plot shown in Figure 7a, and then compared to the pure water case for detailed observation (Figure 7b).

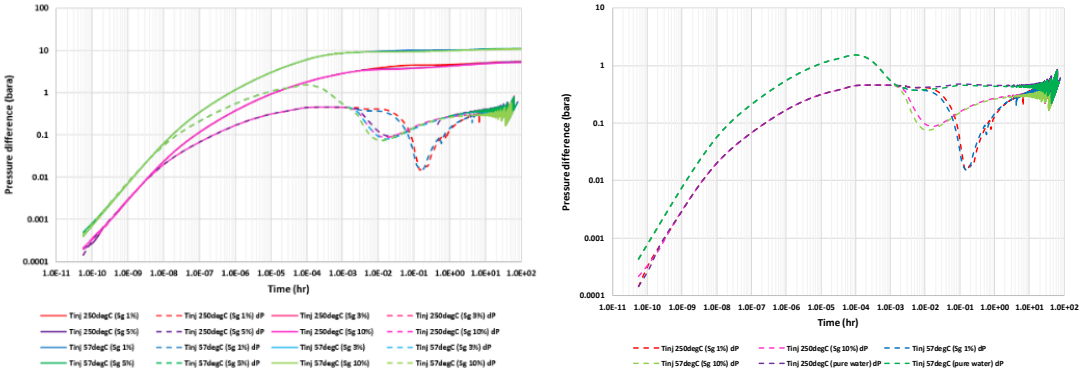

a. **b.**

Figure 7: Effect of gas saturation and injectate temperature on the pressure derivative plot in a reservoir (no-skin) extending infinitely with free CO_2 gas; a. gas saturation variation; b. comparison of gas saturation 1%, 10% to the pure water case

Figure 7a shows that the pressure changes and pressure derivatives for both injectate temperatures are similar. Although pressure differences (and pressure derivatives) are higher for cold water injection cases, they follow a similar trend (for example, at 1% gas saturation, the pressure derivative drops to between 0.1 and 1 log hour for both injectate temperatures). It shows that the diagnostic plot exhibits similar characteristic behavior even if the injection temperatures are different. This also indicates that the cooling effects of cold-

water injection do not exhibit any significant difference in the diagnostic plot at the early times of the fall-off period. Also, because the injected water has a different phase from the reservoir fluid, it forms a moving thermal front. As shown in Kaya et al. (2019), cold water injection makes the steam condense (or CO_2 dissolved in water), resulting in a pressure drop. It also shows that initial reservoir gas saturation has no significant influence on the diagnostic plot, apart from the late time behavior of the Sg=1.0% case, as both pressure and derivative plots show identical behavior.

To analyze in detail, the pressure derivative in the fall-off period is replotted by comparing 1% gas saturation, 10% gas saturation, and pure water for all injected temperatures and shown in Figure 7b. For both injection temperatures, the flat-line of the IARF region is only continuously visible for the pure water case. For the cases that the reservoir has initially low free-CO_2 (Sg=1.0%), the derivative plot shows a short-term IARF region and then deviates from the flat line. For high Sg values (Sg=10%) there is no apparent IARF region observed. For the cold-water injection case, the derivative plot starts to dive earlier (as observed in Figure 7b). Interestingly, the temperature difference strongly influences the IARF region reached. After that, the derivative values become similar for both reinjection temperatures, and they only vary for initial gas saturation values.

While Sg=3%, 5%, and 10% cases show similar values for the derivatives, the different behavior of 1% gas saturation is due to the condensation front. The condensation front of the low-gas saturation case is likely to advance farther into the formation due to the small volume fractions of gas in the reservoir fluid**.** Figure 8 shows the condensation front at the end of injection and at the end of fall-off periods for the injectate temperature of 250°C.

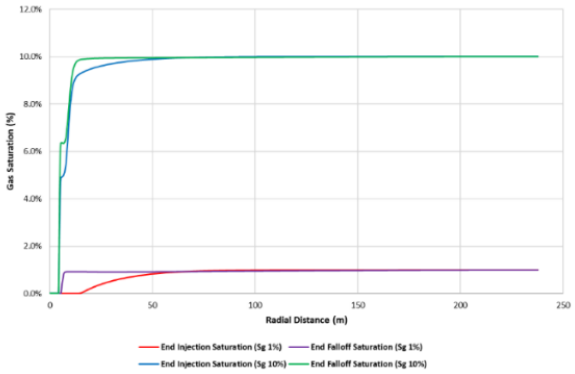

Figure 8: Radius of condensation front between gas saturation 1% and 10%

For the 1% gas saturation case, the condensation front at the end of the injection period reached 14.2 m. However, during the fall-off period, the condensation front is reduced to 5.38 m. This is due to the high compressibility of two-phase fluid beyond the thermal front is compressing the single-phase fluid located in the condensation front region. This results in the high-pressure drop at the intermediate times in the fall-off period. On the other hand, for 10% gas saturation, the condensation front remains the same at the end of the injection and fall-off period. The difference in pressure derivative of 1% gas saturation can also be due to immobile gas saturation, which will be analyzed in detail in the next section.

Table 7: Reservoir parameters estimated for different gas saturation and injectate temperature in a reservoir (no-skin) extending infinitely with free CO_2 gas

Injectate Temperature (°C)	S_g	k (mD)	Δk (mD)	Skin	ΔSkin
57	1%	11.44	1.44	8.38	8.38
	3%	11.23	1.23	7.79	7.79
	5%	11.72	1.72	7.73	7.73
	10%	12.85	2.85	7.82	7.82
250	1%	9.87	0.13	0.42	0.42
	3%	10.12	0.12	0.41	0.41
	5%	10.4	0.4	0.4	0.4
	10%	11.14	1.14	0.31	0.31

Table 7 summarizes the estimation of reservoir properties using Horner and semilog plots. The reservoir permeability estimated is barely different from the actual value, but it is quite different in a 10% gas saturation for both injectate temperatures. The derived skin factor value in injectate temperature 250°C shows no significant difference from the actual value. In the case of injectate temperature is 57°C, the skin factor value calculated is overestimated.

4.1.2 Infinite reservoir with positive and negative skin

The effect of positive and negative skin is investigated, and the result of pressure derivative and estimation of reservoir parameters are shown in Figure 9 and Table 8.

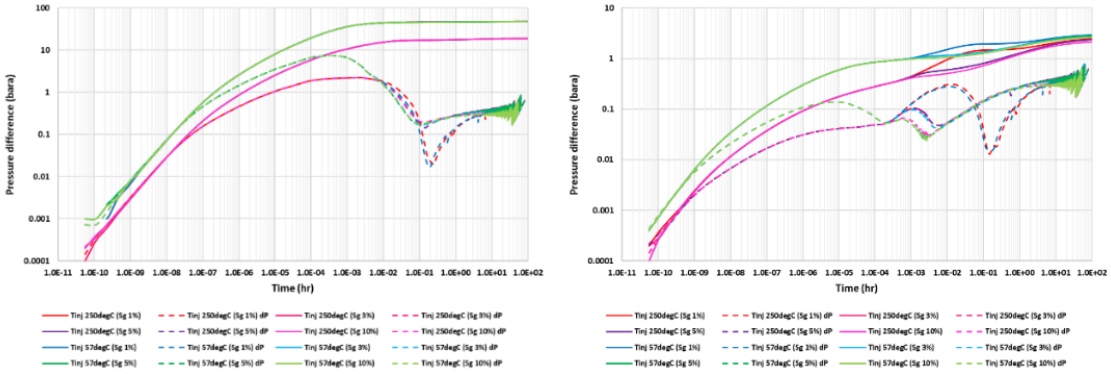

a. **b.**

Figure 9: Effect of gas saturation, injectate temperature, and skin factor value on the pressure derivative plot in a reservoir with skin zone extending infinitely with free CO_2 gas; a. positive skin; b. negative skin

Table 8: Reservoir parameters estimated for different gas saturation, injectate temperature, and skin factor value in the reservoir with skin zone extending infinitely with free CO_2 gas

Actual skin factor value	Injectate Temperature (°C)	S_g	k (mD)	Δk (mD)	Skin	ΔSkin
14.63 (positive skin)	57	1%	13.58	3.58	65.14	50.51
		3%	13.88	3.88	63	48.37
		5%	14.14	4.14	63.66	48.37
		10%	13.95	7.95	75.66	61.03
	250	1%	13.47	3.47	19.97	5.34
		3%	12.94	2.94	19.06	4.43
		5%	13.73	3.73	18.93	4.3
		10%	17.43	7.43	22.88	8.25
-3.29 (negative skin)	57	1%	13.59	3.59	-3.26	0.03
		3%	13.89	3.89	-3.53	0.24
		5%	14.34	4.34	-3.68	0.39
		10%	18.29	8.29	-3.18	0.11
	250	1%	13.16	3.16	-4.08	0.79
		3%	13.03	3.03	-4.71	1.42
		5%	13.75	3.75	-4.63	1.34
		10%	17.52	7.52	-4.02	0.73

For the positive skin factor value, the result illustrates that the high-pressure change appeared as a bigger hump than in the no-skin reservoir case (Figure 9a). It also shows that gas saturation has no significant effect on the behavior of derivative plots when there is positive skin around the well, as similar behavior obtained to the derivative plots shown in Figure 7a. In the negative skin model, several humps occur in the derivative value (Figure 9b). For the detailed investigation, the pressure derivative plot will be divided for injectate temperature 57°C and 250°C (Figure 10).

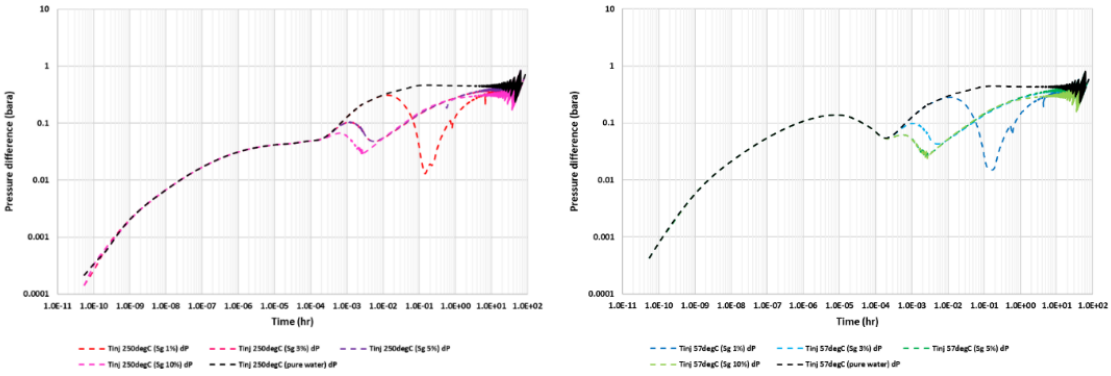

a. **b.**

Figure 10: Pressure derivative plot (derivative only) in a negative skin and reservoir zone extending infinitely; a. injectate temperature of 250°C; b. injectate temperature of 57°C

At first, it should be noted that the skin zone has higher permeability than the reservoir, resulting in a lower pressure difference during the transitional zone. However, the small hump still occurred in the cold-water injection due to the high viscosity of cold-water injection. In the 1% gas saturation case, the derivative pressure was eventually similar to the pure water case. However, at 0.01 log hour, the gas

dissolves in water, resulting in a high decrease of the derivative pressure. For 3%, 5%, and 10% gas saturation, the gas condensation occurred earlier time (at 0.001 log hours) than 1% gas saturation with 10% gas saturation being the earliest among others. The decrease of derivative pressure is close for 3%, 5%, and 10% gas saturation cases. The estimation of reservoir permeability (summarized in Table 8) seems to have a quite high error value for 10% gas saturation and other saturation values. The estimated skin value is greatly exaggerated for cold water injection.

4.1.3 Reservoir with closed and constant pressure boundary

This section investigates the effect of closed and constant pressure boundaries in the two-phase reservoir. The two-phase compressibility is higher than the single-phase compressibility, may be orders of magnitude larger than its single-phase equivalent. The kinematic viscosity for a two-phase mixture is not different for either liquid or steam. This means that the two-phase diffusivity is very small, and the pressure changes spread extremely slowly in the reservoir (O'Sullivan & McKibbin, 1989). Thus, in simulating the boundary condition, the extent of the reservoir is reduced to 50 m to make the boundary effect more pronounced. For the constant pressure boundary condition, an aquifer zone is added with a radius extent of 20 m. The pressure derivative plot and the result of reservoir parameters are shown in Figure 11 and Table 9.

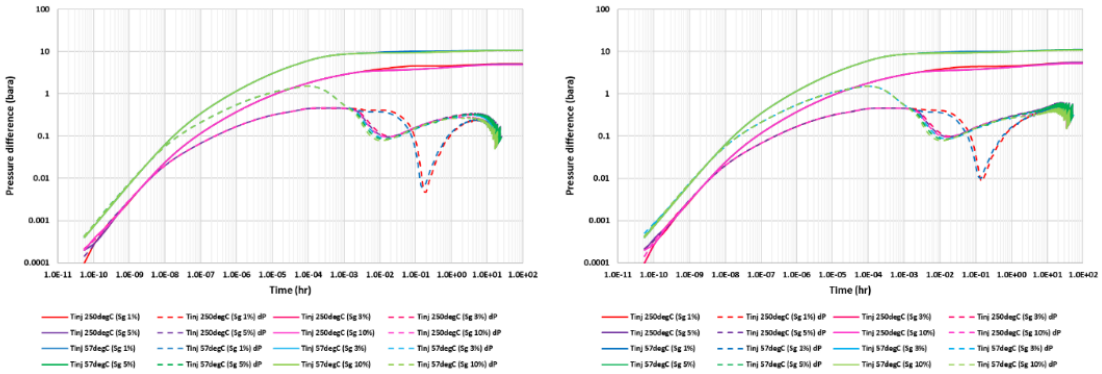

a. **b.**

Figure 11: Effect of gas saturation, injectate temperature, and boundary conditions on the pressure derivative plot in reservoir zone with free CO_2 gas; a. closed or no flow boundary; b. constant pressure boundary

Table 9: Reservoir parameters estimated for different gas saturation, injectate temperature, and boundary conditions in the reservoir zone with free CO_2 gas

Boundary condition	Injectate Temperature (°C)	S_g	k (mD)	Δk (mD)	Skin	ΔSkin
Closed boundary	57	1%	11.91	1.91	8.75	8.75
		3%	12.56	2.56	9.03	9.03
		5%	12.31	2.31	8.97	8.97
		10%	14.29	4.29	9.26	9.26
	250	1%	9.83	0.17	0.48	0.48
		3%	10.08	0.08	0.46	0.46
		5%	10.38	0.38	0.44	0.44
		10%	11.11	1.11	0.49	0.49
Constant pressure boundary	57	1%	12.03	2.03	8.85	8.85
		3%	12.56	2.56	8.95	8.95
		5%	12.31	2.31	8.4	8.4
		10%	14.29	4.29	9.17	9.17
	250	1%	9.85	0.15	0.46	0.46
		3%	10.09	0.09	0.39	0.39
		5%	10.38	0.38	0.39	0.39
		10%	11.11	1.11	0.3	0.3

For both boundary conditions, the pressure derivative dives towards zero at the late times, representing the pseudo-steady state flow. The derivative pressure of 1% gas saturation drops significantly compared to other gas saturations due to the condensation front. The variation of the injection mass flow rate does not significantly impact the time when the constant pressure boundary is felt. The reservoir parameter estimation for uniform reservoirs with the closed and constant pressure boundary is shown in Table 9. As can be seen from this table, varying the gas saturation impact affects the accuracy of the permeability estimation; the higher the gas saturation, the bigger difference between the derived permeability to the actual permeability. For skin factor value, gas saturation variation does not significantly impact the accuracy of the derived skin factor value.

4.2 Effect of Relative Permeability

For two-phase flow, the concept of relative permeability is important, because liquid and steam (or gas) phases interfere with each other and may cause a reduction in flow capability as they move through the rock. At high gas saturation, the gas phase will flow easily (higher permeability), while the flow of the water phase will be dependent on the immobile water saturation. Similarly, at high water saturation, the flow of water and gas will be dependent on immobile gas saturation.

In this study, the linear relative permeability curve is used. The residual liquid saturation (immobile liquid saturation, S_l) is 0.30, and the residual gas saturation (immobile gas saturation, S_v) is varied between 0.0, 0.03, 0.05, and 0.1. The gas-phase saturation, S_g, is kept at 3%. However, 1% gas saturation will also be simulated in the uniform and infinite reservoir model to analyze the peculiar behavior further.

4.2.1 Infinite reservoir with no skin

The experiment was conducted by varying immobile gas saturation in the uniform and infinite reservoir model. The derivative plot during the fall-off period is shown in Figure 12a, and the calculated reservoir parameters are summarized in Table 10. The relative permeability effect on the two-phase reservoir that initially has 1% gas saturation and 3% gas saturation is also simulated. The result of the derivative plot is shown in Figure 12b.

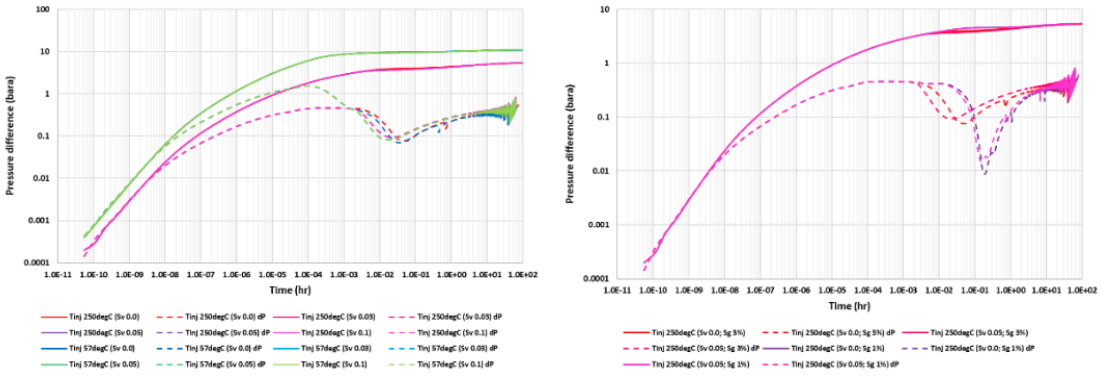

a. b.

Figure 12: Effect of relative permeability and injectate temperature on the pressure derivative plot in a reservoir (no-skin) extending infinitely with free CO_2 gas; a. relative permeability variation; b. comparison of gas saturation 1% and 3% with different relative permeability

Table 10: Reservoir parameters estimated for different relative permeability and injectate temperature in a reservoir (no-skin) extending infinitely with free CO_2 gas

Injectate Temperature (°C)	S_v	k (mD)	Δk (mD)	Skin	ΔSkin
57	0.0	11.32	1.32	7.76	7.76
	0.03	11.25	1.25	7.8	7.8
	0.05	11.27	1.27	7.82	7.82
	0.1	10.71	0.71	7.33	7.33
250	0.0	10.15	0.15	0.43	0.43
	0.03	10.18	0.18	0.42	0.42
	0.05	10.09	0.09	0.4	0.4
	0.1	10.09	0.09	0.4	0.4

Figure 12a illustrates that the pressure derivative falls, and then the curve reaches the horizontal line. The horizontal line is likely representing the IARF. Although the injection temperature difference initially influences the derivative plots, this difference diminishes when it has reached the IARF region. For both injectate temperatures, the derivative pressure gives a slightly delayed response for the Sv=0.0 case, relative to other immobile gas saturation values (Sv=0.03, 0.05, 0.1) that demonstrate identical behaviors. The reservoir parameters estimated have a quantified error below 15%. But the skin factor value is overestimated for cold water injection case (Table 10).

Figure 12b shows that the relative permeability does not significantly impact how much the pressure derivative decreases. The reservoir that initially has 1% gas saturation still has a huge drop in the derivative pressure. Variation of immobile gas saturation only slightly shifts when the pressure drop occurs.

4.2.2 Infinite reservoir with positive and negative skin

The effect of relative permeability is simulated in a reservoir that has positive and negative skin with free CO_2 gas. The pressure derivative plot results are shown in Figure 13a, Figure 13b, and the estimation of reservoir parameters are tabulated in Table 11.

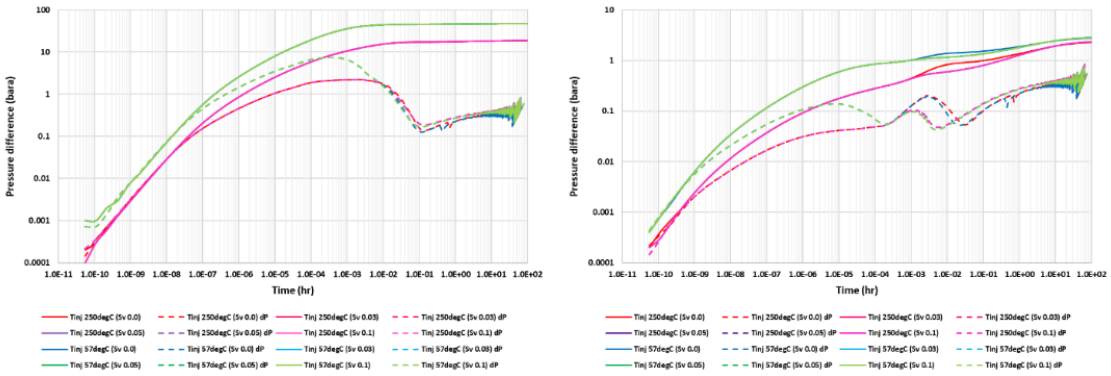

a. b.

Figure 13: Effect of relative permeability, injectate temperature, and skin factor value on the pressure derivative plot in a reservoir with skin zone extending infinitely with free CO_2 gas; a. positive skin; b. negative skin

Table 11: Reservoir parameters estimated for different relative permeability, injectate temperature, and skin factor value in the reservoir with skin zone extending infinitely with free CO_2 gas

Actual skin factor value	Injectate Temperature (°C)	S_v	k (mD)	Δk (mD)	Skin	ΔSkin
14.63 (positive skin)	57	0.0	15.8	5.8	72.75	58.12
		0.03	13.87	3.87	64.45	49.82
		0.05	14.15	4.15	65.8	51.17
		0.1	13.91	3.91	63.91	49.28
	250	0.0	15.31	5.31	23.64	9.01
		0.03	13.04	3.04	19.22	4.59
		0.05	13.5	3.5	19.97	5.34
		0.1	13.52	3.52	20	5.37
-3.29 (negative skin)	57	0.0	15.74	5.74	-3.17	0.12
		0.03	13.87	3.87	-3.22	0.07
		0.05	14.12	4.12	-3.55	0.26
		0.1	13.89	3.89	-3.45	0.1
	250	0.0	15.26	5.26	-3.79	0.5
		0.03	13.07	3.07	-4.44	1.15
		0.05	13.49	3.49	-4.51	1.22
		0.1	13.16	3.16	-4.53	1.24

The positive skin results in a higher hump on the derivative plot. Several humps are seen in the derivative plot in the negative skin model due to the permeability and injectate temperature difference. Variation of immobile gas saturation only affects the time at which the pressure drops. However, the difference in time is not significant. The estimation of reservoir parameters is much different from the actual value, especially for the injectate temperature at 57°C (Table 11). The reservoir permeability and skin factor value deduced from the Horner plot are slightly overestimated.

4.2.3 Reservoir with closed and constant pressure boundary

In this section, the effect of closed and constant pressure boundary in the two-phase reservoir is investigated with relative permeability variation. The results are shown in Figure 14 and Table 12.

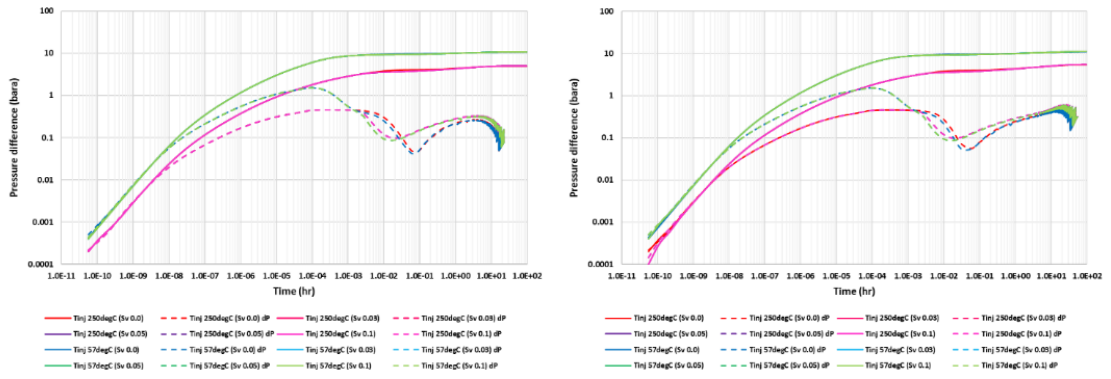

a. b.

Figure 14: Effect of relative permeability, injectate temperature, and boundary condition on the pressure derivative plot in reservoir zone with free CO_2 gas; a. closed or no flow boundary; b. constant pressure boundary

Table 12: Reservoir parameters estimated for different relative permeability, injectate temperature, and boundary conditions in the reservoir zone with free CO_2 gas

Boundary condition	Injectate Temperature (°C)	S_v	k (mD)	Δk (mD)	Skin	ΔSkin
Closed boundary	57	0.0	11.31	1.31	7.81	7.81
		0.03	11.63	1.63	8.07	8.07
		0.05	11.64	1.64	8.21	8.21
		0.1	10.97	0.97	7.49	7.49
	250	0.0	10.16	0.16	0.39	0.39
		0.03	10.23	0.23	0.38	0.38
		0.05	10.1	0.1	0.35	0.35
		0.1	10.1	0.1	0.35	0.35
Constant pressure boundary	57	0.0	11.32	1.32	7.94	7.94
		0.03	11.63	1.63	8.26	8.26
		0.05	11.64	1.64	8.14	8.14
		0.1	10.97	0.97	7.55	7.55
	250	0.0	10.16	0.16	0.38	0.38
		0.03	10.23	0.23	0.43	0.43
		0.05	10.1	0.1	0.4	0.4
		0.1	10.1	0.1	0.4	0.4

The result shows the pressure derivative dives towards zero at the late times during the fall-off period. The variation of immobile gas saturation does not affect the time when the boundary is detected. The result of reservoir properties estimation shows that the accuracy of reservoir properties estimation is not influenced by the immobile gas saturation variation (Table 12). For injectate temperature of 250°C there is a small difference between the reservoir parameter estimated and the actual value, while for an injectate temperature of 57°C, the skin value is overestimated compared to the actual value.

5. CONCLUSIONS

The objectives of this study were to investigate the pressure response behavior of a geothermal reservoir under various conditions (i.e., single-phase pure water and two-phase with free CO_2) for injection fall-off tests and identify the accuracy of the forecasts using commonly used PTA methods. A set of numerical models was carried out to incorporate injection fall-off records and corresponding pressure and temperature responses. Key findings in this study are as follows:

CO_2 content

The presence of the free-CO_2 phase in the geothermal reservoir is found to impact the pressure response of the reservoir. It is illustrated as the decline in the derivative pressure before reaching the IARF. This is because the CO_2 presence in the reservoir dissolves in the water due to the single-phase pure water injection.

Gas saturation

The variation of gas saturation in the reservoir with the free CO_2 phase has affected the derivative plot results. In the low-gas saturation case (Sg=1%), the derivative pressure falls more than the higher gas saturation cases. This is probably due to the condensation front of the low-gas saturation reservoir that advances farther into the formation. The high compressibility of two-phase fluid results in the fluid in the condensation front to experience the high-pressure drop.

Relative permeability (variation of immobile gas saturation)

Changing the immobile gas saturation affects the time at which the pressure drops. Using immobile gas saturation of 0.0 makes the pressure drop occur later than others.

Injectate temperature

The effect of injectate temperature variation is similar to the single-phase model, as the higher the temperature difference, the bigger the hump, which resembles a positive skin.

Skin effect

The effect of positive and negative skin on the pressure derivative plot is similar to the single-phase model. The positive skin will result in a bigger hump than the negative skin.

Boundary condition (closed and constant pressure)

The fluid flows in the free-CO_2 reservoir reach the boundary by reducing the reservoir radius to 50 m which is smaller than the single-phase reservoir model. This is due to the high compressibility of two-phase fluid, making the two-phase diffusivity very small. Hence, the pressure changes spread extremely slowly in the reservoir. The pressure response due to the boundary effect is similar to the single-phase reservoir, represented by the late time unit slope.

REFERENCES

Adityatama, D. W., Kaya, E., & Zarrouk, S. J. (2018a). Investigation of pressure transient analysis methods for single and multiphase geothermal reservoirs. *Proceedings 40th New Zealand Geothermal Workshop*, *November*, 1–8.

Adityatama, D. W., Wisesa, N. O., Purba, D. P., & Kaya, E. (2018b). Utilising TOUGH2 simulator to manage the limitation of current analytical method in geothermal pressure transient analysis. *Proceedings the 6th Indonesia International Geothermal Convention and Exhibition (IIGCE)*, 10.

Battistelli, A., Calore, C., & Pruess, K. (1997). The simulator TOUGH2/EWASG for modelling geothermal reservoirs with brines and non-condensible gas. *Geothermics*, *26*(4), 437–464. https://doi.org/10.1016/S0375-6505(97)00007-2

Bourdet, D., Ayoub, J. A., & Pirard, Y. M. (1989). Use of pressure derivative in well-test interpretation. *SPE Formation Evaluation*, *4*(02), 293–302. https://doi.org/10.2118/12777-pa

Croucher, A. (2011). Pytough: a python scripting library for automating tough2 simulations. *Proceedings of the New Zealand Geothermal Workshop*, *November*, 1–6.

Guerra, R. J. A., & O'Sullivan, J. (2018). Investigating the effects of non-isothermal reservoir conditions on pressure transient analysis of an injection/fall-off test using numerical modelling. *Proceedings 40th New Zealand Geothermal Workshop*, *November*, 1–8.

Houzé, O., Viturat, D., Fjaere, O., & Trin, S. (2012). Dynamic data analysis. In *Kappa Engineering*. Kappa Engineering.

Kaya, E., Adityatama, D., & Zarrouk, S. J. (2019). Investigation of pressure transient analysis methods for single-phase and CO2-rich geothermal reservoirs. *Renewable Energy*, *141*, 162–180. https://doi.org/10.1016/j.renene.2019.03.140

McLean, K., & Zarrouk, S. J. (2017). Pressure transient analysis of geothermal wells: A framework for numerical modelling. *Renewable Energy*, *101*, 737–746. https://doi.org/10.1016/j.renene.2016.09.031

O'Sullivan, M. J., Bodvarsson, G. S., Pruess, K., & Blakeley, M. R. (1983). Fluid and heat flow in gas-rich geothermal reservoirs. *Society of Petroleum Engineers Annual Technical Conference and Exhibition*.

O'Sullivan, Michael J., & McKibbin, R. (1989). Geothermal reservoir engineering. In *The University of Auckland*. https://doi.org/10.1016/C2010-0-64792-4

Onur, M., & Al-Saddique, M. (1999). Comparison of derivative algorithms used in pressure transient analysis. *The Arabian Journal for Science and Engineering*, *24*(1B), 59–78.

Pruess, K., Oldenburg, C., & Moridis, G. (1999). *TOUGH2 User's Guide, Version 2.0 (No. LBNL-43134)* (Issue November).

Septiani, G. A., Kaya, E., & Adityatama, D. W. (2021a). Pressure Transient Analysis of Injection/Fall-off Tests in the Fractured Geothermal Reservoir. *The 2nd Digital Indonesia International Geothermal Convention (DIIGC)*, 1–12.

Septiani, G., Adityatama, D. W., Kaya, E., & Zarrouk, S. J. (2021b). Numerical Pressure Transient Analysis of CO2-Containing Geothermal Reservoirs during Draw-Down Buildup Testing. *World Geothermal Congress 2020+1*, *April-October*, 1–10.

Yeh, A., Croucher, A. E., & Sullivan, M. J. O. (2012). Recent developments in the AUTOUGH2 simulator. *Proceedings TOUGH Symposium*, 8.

Zarrouk, S. J., & McLean, K. (2019). *Geothermal well test analysis* (1st ed.). Elsevier Inc. https://doi.org/https://doi.org/10.1016/C2017-0-02723-4